

Peptide Ketobenzoxazole Inhibitors Bound to Cathepsin K

Mary E. McGrath,* Paul A. Sprengeler, Craig M. Hill, Valeri Martichonok, Harry Cheung, John R. Somoza, James T. Palmer, and James W. Janc

Celera, 180 Kimball Way, South San Francisco, California 94080

Received July 7, 2003; Revised Manuscript Received October 6, 2003

ABSTRACT: Potent inhibitors of human cysteine proteases of the papain family have been made and assayed versus a number of relevant family members. We describe the synthesis of peptide α -ketoheterocyclic inhibitors that occupy binding subsites S1'-S3 of the cysteine protease substrate recognition cleft and that form a reversible covalent bond with the Cys 25 nucleophile. X-ray crystal structures of cathepsin K both unbound and complexed with inhibitors provide detailed information on protease/inhibitor interactions and suggestions for the design of tight-binding, selective molecules.

Cathepsin K (E.C. 3.4.22.38) is a lysosomal cysteine protease of the papain family. It is synthesized as a zymogen, which is processed to remove a 99 residue proregion (1), leaving the active 215 amino acid protease. In nonpathological situations, it is expressed predominantly by the bone-remodeling osteoclast cells. Bone degradation takes place when osteoclasts attach to the bone surface and release protons into the resorption lacunae. These protons demineralize the substrate and reveal the proteinaceous components of bone. Collagenolysis is then accomplished through the activity of cathepsin K, and a pit is formed on the bone surface. The process of bone degradation is balanced by the complementary action of osteoblasts, which rebuild bone. Disequilibrium in the direction of excessive bone breakdown is characteristic of the disease osteoporosis, suggesting that it might be possible to treat this disease by attenuating bone degradation. The possible therapeutic value of cathepsin K inhibition in osteoporotic patients was suggested by numerous lines of evidence. Standard cysteine protease inhibitors such as E-64 and leupeptin curtail osteoclastic bone resorption (2, 3). Inactivating mutations in cathepsin K result in reduced bone turnover and overly dense and easily fracturing bones in the rare disorder known as pycnodysostosis (4). Studies using an antisense oligonucleotide to the coding sequence of cathepsin K showed decreased bone resorption as a function of dose (5), and two laboratories have produced cathepsin K knockout mice exhibiting the characteristic symptoms of osteopetrosis (6, 7).

Active-site directed inhibitors of cathepsin K have been reported by a number of laboratories and feature a variety of electrophiles found to interact with the catalytic Cys 25 (papain numbering system). Irreversible inhibitors include the epoxides, of which E-64 (8) is the most studied, the peptidyl vinyl sulfones (9, 10), and the acyloxymethyl ketones

(11). Inhibitors that bind via a reversible covalent bond to Cys 25 include peptidic aminomethyl ketones (12), diacyl aminoketones (13), alkoxymethyl ketones (14), diaminopyrrolidinones (15), diacylcarbohydrazides (16), azepanones (17), and the nonpeptidic cyanamides (18). Recently, aryl-aminoethyl amides have been documented as noncovalent inhibitors of cathepsin K (19). Apart from contacts with the catalytic machinery of these enzymes, cysteine protease inhibitors usually occupy more than one of the linearly arranged substrate-binding subsites. Those sites are characterized by available hydrogen bonding partners for peptide substrate carbonyl and amide groups and pockets of varying size, shape, and discrimination tailored for side chains of substrate amino acids. Some inhibitor classes sample only the nonprime side of the substrate binding cleft, while others extend beyond the catalytic ion pair to interact with subsites beyond the scissile bond. Herein we describe covalent, reversible inhibitors that provide potency and selectivity elements on both the prime and the nonprime sides of the substrate-binding cleft.

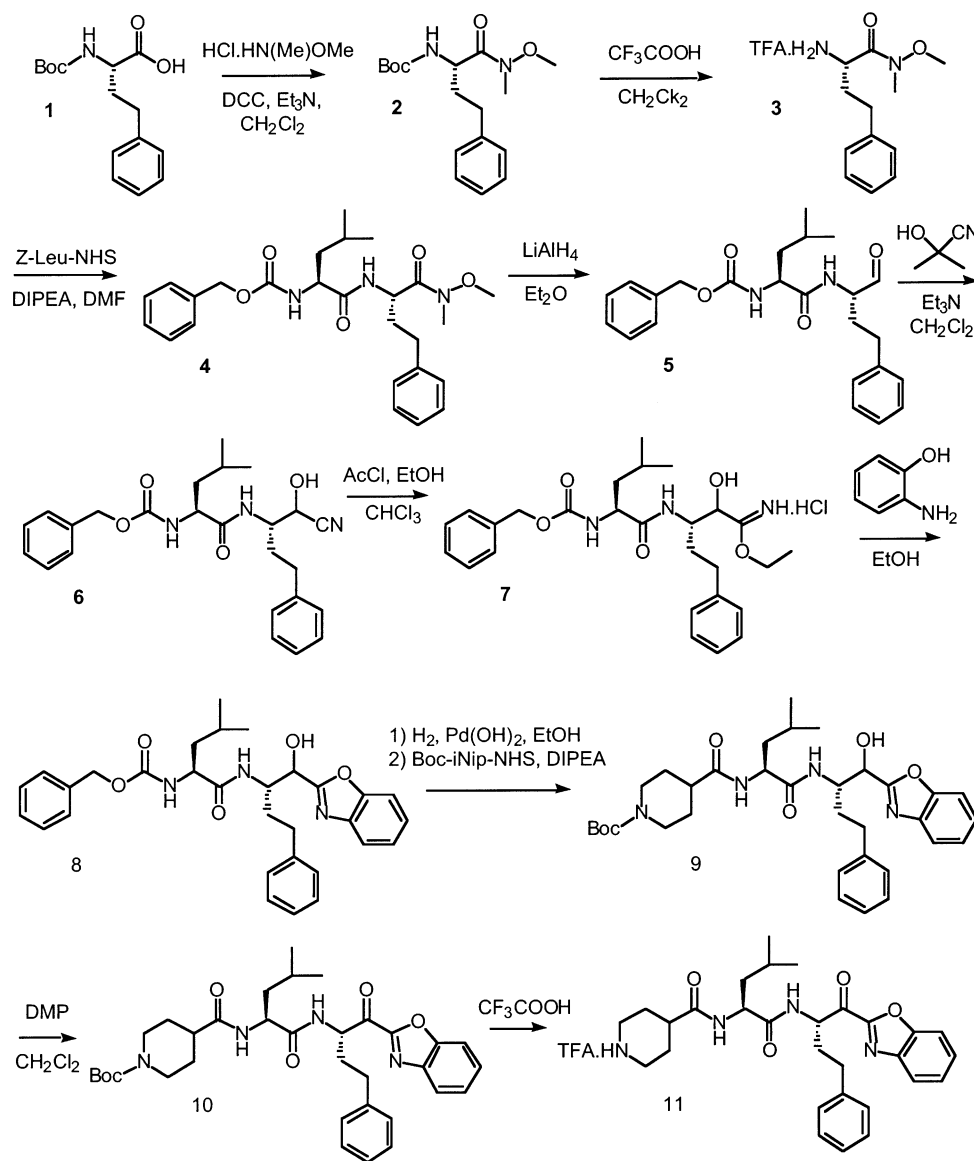
EXPERIMENTAL PROCEDURES

Preparation of recombinant human cathepsins K (20), S (21), V (22), and F (23) has been described previously. Human cathepsins B and L were obtained from Athens Research and Technology (Athens, GA). The substrates Cbz-Phe-Arg-AMC,¹ Boc-Leu-Lys-Arg-AMC, and Cbz-Val-Val-Arg-AMC were purchased from Bachem (King of Prussia, PA). Bovine serum albumin, DTT, and MES (free acid) were purchased from Sigma Chemical Company (St. Louis, MO).

¹ Abbreviations: AMC, 7-amino-4-methylcoumarin; Boc, *tert*-butoxycarbonyl; BSA, bovine serum albumin; Cbz, benzyloxycarbonyl; DMSO, dimethyl sulfoxide; DTT, D,L-dithiothreitol; E-64, *L*-trans-(epoxysuccinyl)leucylamido(4-guanidino)butane; EDTA, ethylenediaminetetraacetic acid; MES, 4-morpholine-ethanesulfonic acid; RFU, relative fluorescence unit; MPD, 2-methyl-2,4-pentandiol; Tris, tris(hydroxymethyl)aminomethane hydrochloride; NaOAc, sodium acetate.

* Corresponding author. Tel: (650) 866-6597. E-mail: mary.mcgrath@celera.com.

Scheme 1



All other reagents used in this study were of the highest quality and purity available.

Compound Synthesis. CRA1—morpholine-4-carboxylic acid [1-(3-benzenesulfonyl-1-phenethyl-allylcarbamoyl)-2-(4-hydroxyphenyl)ethyl]-amide (Mu-Tyr-HphVSPH).

This compound was prepared as published (9). ^1H NMR (CDCl_3): 1.68 (1H, m), 1.81 (1H, m), 1.93 (2H, m), 2.52 (2H, m), 2.9 (2H, m), 3.28 (4H, m), 3.58 (4H, m), 4.48 (1H, m), 4.58 (1H, m), 5.36 (1H, m), 5.89 (1H, d, $J = 16$ Hz, *trans*-vinyl sulfone CH), 6.64 (1H, d*), 6.66 (2H, d), 6.97 (2H, d), 7.01 (2H, d), 7.05–7.23 (3H, m), 7.5 (2H, m), 7.58 (1H, m), 7.84 (2H, m).

CRA3 (iNip-Leu-Hph-ketobenzoxazole, (*S,S*)-piperidine-4-carboxylic acid {1-[1-(benzoxazole-2-carbonyl)-3-phenylpropylcarbamoyl]-3-methyl-butyl}-amide) (**11**) is shown in Scheme 1. Treatment of Boc-homophenylalanine (**1**) with *N,O*-dimethylhydroxylamine hydrochloride in the presence of DCC and triethylamine in dichloromethane afforded the Weinreb amide (**2**). This material was deprotected by means of TFA in dichloromethane to give **3** and was coupled with CBZ-leucyl-*N*-hydroxysuccinimide in the presence of di-

isopropylethylamine in DMF. The product, **4**, was isolated by being poured into ice water, filtered, washed several times with cold water, and dried in vacuo over P_2O_5 , in 93% overall yield.

To a suspension of lithium aluminum hydride (36 mg, 0.9 mmol) in ether (6 mL) at -45°C was added a solution of **4** (315 mg, 0.67 mmol) in ether (6 mL) over 5 min while maintaining cooling. The cooling bath was removed, and the mixture was permitted to warm to 5°C . The solution was then cooled once more to -35°C , and a saturated solution of NaHSO_4 (0.3 mL) was added carefully. The temperature was allowed to rise to 0°C , the cooling bath was removed, and the mixture was stirred at room temperature for 1 h. The mixture was filtered, the solids were washed with ether (50 mL), and the combined organics were washed with cold 1 M HCl (2×10 mL), saturated aqueous NaHCO_3 (2×10 mL), brine (10 mL) and dried over Na_2SO_4 , filtered, and concentrated in vacuo to give a colorless oil. The yield of **5** was 234 mg (87%).

A solution of **5** (2.75 g, 6.7 mmol) in CH_2Cl_2 (30 mL) was purged with nitrogen and was treated with acetone

cyanohydrin (1.84 mL, 20.1 mmol), followed by triethylamine (0.546 mL, 4.0 mmol) and stirred at room temperature for 4 h. The solvent was evaporated. The residue was dissolved in ether (150 mL), washed with brine (5 × 20 mL), dried over MgSO₄, filtered, and evaporated. The resulting crude cyanohydrin was purified by chromatography on silica gel, using 1:1 ethyl acetate/hexane as mobile phase, affording 1.93 g (66%) of the product **6**. A solution of anhydrous ethanol (1.22 mL, 30.7 mmol) in chloroform (2 mL) at 0 °C was treated with acetyl chloride (1.24 mL, 17.4 mmol) followed by a solution of **6** (0.5 g, 1.09 mmol) in chloroform (3 mL). The mixture was allowed to warm to ambient temperature and was stirred overnight. The solvent was evaporated, and the crude imidate ester **7** (weight: 0.51 g) was dried in vacuo to be used in the next step without further purification.

A mixture of **7** (0.51 g, 1.00 mmol) and 2-aminophenol (0.100 g, 1.00 mmol) was dissolved in ethanol (5 mL) and heated at 80 °C for 5 h. The progress of the reaction was monitored by TLC (ethyl acetate/hexane, 1:1). After cooling, the solution was diluted with ethyl acetate (50 mL), washed with brine, dried over MgSO₄, filtered, and concentrated in vacuo. Chromatography on silica gel (mobile phase, 1:1 ethyl acetate/hexane) afforded **8** as a mixture of diastereomers that could be crystallized from ethyl acetate and hexane to give 125 mg (24% yield).

A total of 56 mg (0.11 mmol) of **8** was dissolved in ethanol (3 mL), and 20% palladium hydroxide (15 mg) was added. The solution was exposed to hydrogen in a balloon for 1 h. The reaction mixture was filtered and concentrated in vacuo. To this residue was added Boc-isonipecotiny *N*-hydroxy-succinimide (Boc-iNip-NHS: 48.5 mg, 0.15 mmol). The flask was purged with N₂, the contents were dissolved in DMF (3 mL), the mixture was cooled to 0 °C, and diisopropylethylamine (DIPEA: 0.026 mL, 0.15 mmol) was added. The mixture was stirred overnight, diluted with ethyl acetate (30 mL), washed with 1 M HCl, saturated NaHCO₃, and brine, dried over MgSO₄, filtered, concentrated, and purified by flash chromatography to give 47.2 mg of **9** in 74% overall yield.

A total of 46.3 mg (0.076 mmol) of the hydroxybenzoxazole **9** was then dissolved in dry CH₂Cl₂ (4 mL). Dess–Martin periodinane (64.4 mg, 0.152 mmol) was added. After 30 min, wet CH₂Cl₂ (prepared by dissolution of 0.09 mL of water in 10 mL of CH₂Cl₂) was added dropwise. The mixture became cloudy; TLC (3:1 ethyl acetate/hexane) indicated that the starting material had disappeared. The reaction mixture was diluted with ethyl acetate (50 mL) and washed with saturated NaHCO₃ and 10% Na₂SO₃ (1:1), water, and brine. The organic phase was dried over MgSO₄, filtered, concentrated, and purified to give the ketone by elution on silica gel using 1:1 ethyl acetate/hexane. The yield of **10** was 32.1 mg (67%). This material was dissolved in CH₂Cl₂ (3 mL), and anisole (0.06 mL) was added. The mixture was cooled to 0 °C, and trifluoroacetic acid (4 equiv) was added. The mixture was stirred for 30 min and concentrated in vacuo to give a white solid that was precipitated from CH₂Cl₂/ether twice, giving 19.9 mg (42% overall from the hydroxybenzoxazole) of the product, **11**, M⁺ 505.

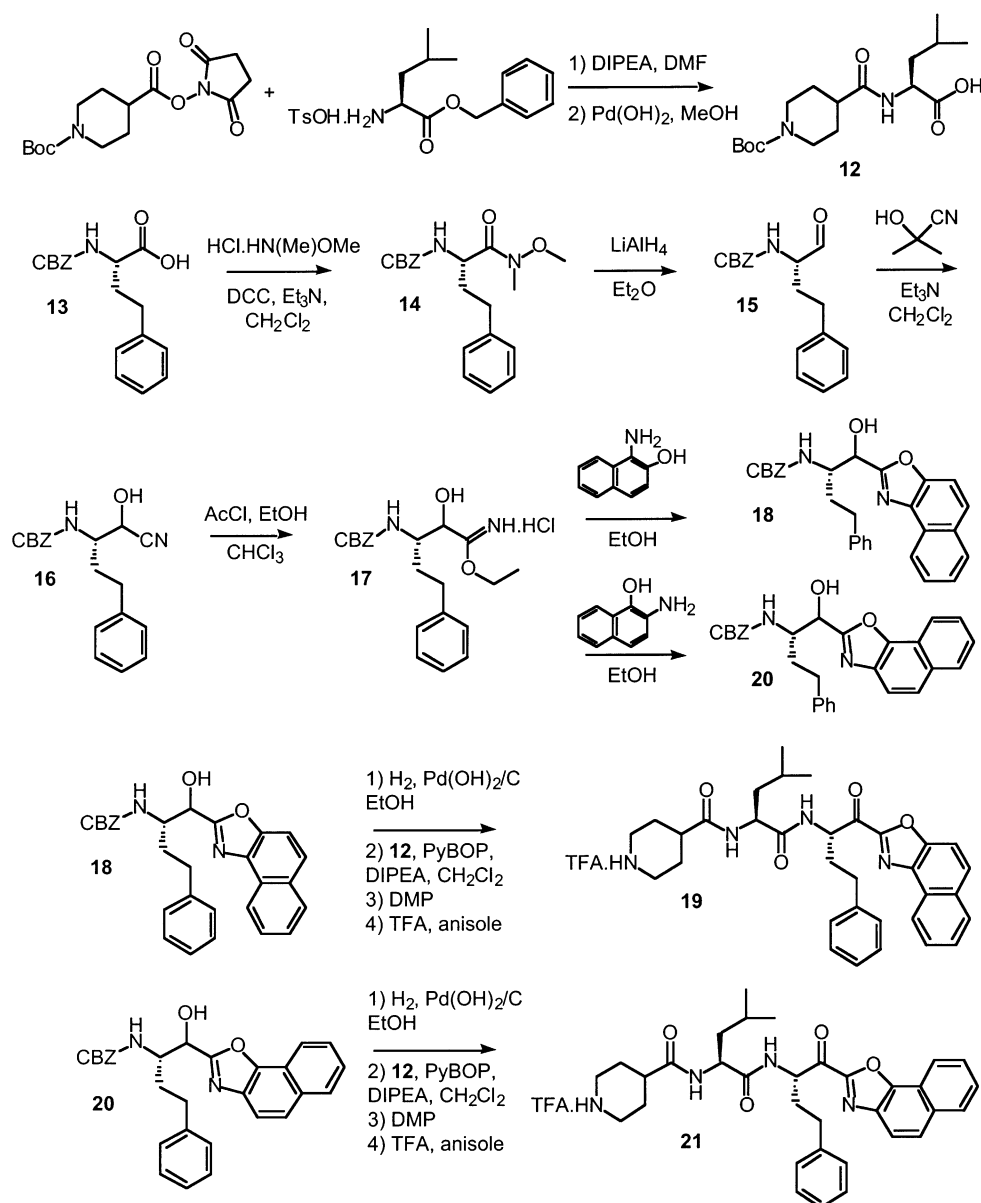
CRA4–piperidine-4-carboxylic acid {3-methyl-1-[1-(naphtho[1,2-d]oxazole-2-carbonyl)-3-phenyl-propylcarbamoyl]-butyl}-amide trifluoroacetate (**19**) is shown in Scheme 2).

A solution of Boc-iNip-NHS (4.25 g, 13 mmol) and benzylleucinate toluenesulfonate (5.13 g, 13 mmol) in DMF (70 mL) was cooled to 0 °C in an ice/water bath. Diisopropylethylamine (5.48 mL, 27 mmol) was added dropwise. The mixture was stirred at 0 °C for 30 min, allowed to warm to room temperature, and then was stirred for an additional 4 h. The mixture was diluted with ethyl acetate (200 mL) and washed with water, 1 M HCl, saturated NaHCO₃, and brine. The solution was dried over MgSO₄, filtered, concentrated, and purified by column chromatography (2:1 hexane/ethyl acetate) to afford 5.61 g (>99%) of the intermediate benzyl ester. This material was dissolved in methanol (200 mL), to which 100 mg of 20% palladium hydroxide on carbon was added. The mixture was hydrogenated, filtered, and concentrated in vacuo to give compound **12**.

CBZ-homophenylalanine, **13**, was converted to its Weinreb amide (*N,O*-dimethylhydroxamate, **14**) and subsequently to the aldehyde **15** by the method outlined in Fehrentz and Castro (24) and described in the synthesis of CRA3. Compound **15** was then converted to the cyanohydrin **16** as described in the synthesis of **11** above. A solution of anhydrous ethanol (30.15 mL, 512 mmol) in chloroform (30 mL) was cooled to 0 °C and treated with acetyl chloride (33 mL, 464 mmol) added dropwise over 15 min. A solution of **16** (5.1 g, 15.53 mmol) in chloroform (20 mL) was added dropwise. The mixture was allowed to warm to room temperature and was stirred overnight. The solvents were removed under reduced pressure, and the residue was dried by coevaporation with anhydrous toluene under reduced pressure. The imidate ester, **17**, was dried in vacuo and used without further purification.

A mixture of **17** (2.03 g, 5 mmol) and 1-amino-2-naphthol (1.59 g, 10 mmol) was dissolved in chloroform (20 mL) and heated at 60 °C for 3 h. The mixture was cooled and concentrated to give the cyclized naphthoxazole, **18**. This material was purified by chromatography (hexane/ethyl acetate), yielding a mixture of diastereomers (yield, 194 mg (8.4%)), which was taken up in ethanol (5 mL), treated with 20% Pd(OH)₂/C (80 min), hydrogenated for 2 h to cleave the CBZ group, and concentrated to give the free amine in 50% yield. This material was combined with **12** (71.8 mg, 0.21 mmol), PyBop (120 mg, 0.24 mmol), and diisopropylethylamine (0.04 mL, 0.23 mmol) in dichloromethane (5 mL), stirred overnight at room temperature, diluted with ethyl acetate (30 mL), washed with 1 M HCl, saturated NaHCO₃, and brine, dried over MgSO₄, filtered, concentrated, and purified by flash chromatography (40% ethyl acetate/hexane) to give 86 mg (62%) of the coupled hydroxybenzoxazole. A total of 76 mg (0.12 mmol) of this compound was dissolved in dichloromethane (5 mL). Dess–Martin periodinane (102 mg, 0.24 mmol) was added. After 30 min, wet CH₂Cl₂ (prepared by dissolution of 0.09 mL of water in 10 mL of CH₂Cl₂) was added dropwise. The mixture became cloudy; TLC (3:1 ethyl acetate/hexane) indicated that the starting material had disappeared. The reaction mixture was diluted with ethyl acetate (50 mL), washed with saturated NaHCO₃ and 10% Na₂SO₃ (1:1), water, and brine. The organic phase was dried over MgSO₄, filtered, concentrated, and purified by elution on silica gel using 1:1 ethyl acetate/hexane to give the ketone, 67 mg, in 88% yield. Last, this material (56 mg) was dissolved in dichloromethane (3 mL). Anisole (0.03 mL) was added. The mixture was cooled to 0

Scheme 2



°C, and trifluoroacetic acid (4 equiv) was added. The mixture was stirred for 30 min and concentrated in vacuo to give a white solid that was precipitated from CH₂Cl₂/ether twice. The yield of **19** was 49 mg (86%). NMR (¹H, *d*₆-DMSO, 400 MHz): 0.79 (3H, d, *J* = 6.4 Hz); 0.80 (3H, d, *J* = 6.4 Hz); 1.42 (2H, m); 1.55 (1H, m); 1.66–1.86 (4H, m); 2.04 (1H, m); 2.34 (1H, m); 2.46 (1H, m*); 2.74–2.9 (4H, m); 3.25 (2H, m); 4.39 (1H, m), 5.26 (1H, m); 7.18–7.32 (5H, Hph-Ar); 7.67 (1H, t, *J* = 7 Hz); 7.80 (1H, t, *J* = 7 Hz); 7.98 (1H, d, *J* = 8 Hz); 8.07 (1H, d, *J* = 8 Hz); 8.16 (2H, d, *J* = 10 Hz); 8.36 (1H, d, *J* = 8 Hz); 8.26, 8.56 (1H, 2 × br s); 8.73 (1H, d, *J* = 7 Hz). MS (*M*⁺: *M* + H): 555.

CRA5-piperidine-4-carboxylic acid {3-methyl-1-[1-(1-oxa-3-aza-cyclopenta[*a*]naphthalene-2-carbonyl)-3-phenyl-propylcarbamoyl]-butyl}-amide trifluoroacetate (**21**) is shown in Scheme 2. A mixture of the previously described imidate **17** (2.03 g, 5 mmol) and 2-amino-1-naphthol (1.59 g, 10 mmol) was dissolved in chloroform (20 mL) and heated at 60 °C for 3 h. The mixture was cooled and concentrated to give the cyclized naphthoxazole, **20**. This material was

purified by chromatography (hexane/ethyl acetate), yielding a mixture of diastereomers, which was taken up in ethanol, treated with 20% Pd(OH)₂/C, hydrogenated for 2 h to cleave the CBZ group, and concentrated to give the free amine. A similar procedure to that used for **19** was employed in converting this material to the final product, **21**. NMR (¹H, *d*₆-DMSO): 0.79 (3H, d, *J* = 6.4 Hz), 0.81 (3H, d, *J* = 6.4 Hz), 1.41 (2H, m), 1.62–1.85 (4H, m), 2.03 (1H, m), 2.29 (1H, m), 2.46 (1H, m*), 2.68–2.9 (4H, m), 3.25 (2H, m), 4.40 (1H, m), 5.25 (1H, m), 7.16–7.3 (5H, m, Hph-Ar), 7.72 (1H, dt, *J* = 7.1, 1 Hz), 7.77 (1H, dt, *J* = 7.1, 1 Hz), 7.95 (1H, d, *J* = 9 Hz), 8.03 (1H, d, *J* = 9 Hz), 8.05 (1H, d*, *J* = 8 Hz), 8.17 (1H, d, *J* = 8 Hz), 8.26 (1H, d, *J* = 8 Hz), 8.21, 8.48 (1H, 2 × br s), 8.75 (1H, d, *J* = 6.4 Hz). MS: (*M*⁺: *M* + H): 555.

K_i' Determinations. Typical human cathepsin K, mutant rabbit cathepsin K, and human cathepsin L inhibition studies were performed in 50 mM MES (pH 5.5), 2.5 mM EDTA, 2.5 mM DTT, and 10% DMSO. The substrate used to monitor cathepsin K and L activity was Cbz-Phe-Arg-AMC.

In both cases, the substrate concentration was fixed at the K_m (40 μ M for cathepsin K and 10 μ M for cathepsin L). Cathepsin B inhibition studies were performed in 50 mM MES (pH 6.0), 2.5 mM EDTA, 2.5 mM DTT, 0.001% Tween-20, and 10% DMSO. The substrate used to monitor cathepsin B activity was Boc-Leu-Lys-Arg-AMC (supplied at the K_m , 190 μ M). Cathepsin S inhibition studies were performed in 50 mM MES (pH 6.5), 2.5 mM EDTA, 100 mM NaCl, 2.5 mM 2-mercaptoethanol, 0.001% BSA, and 10% DMSO. The substrate used to monitor cathepsin S activity was Cbz-Val-Val-Arg-AMC (supplied at the K_m , 60 μ M). Typically, the evaluation of a given inhibitor's potency was determined with the cathepsin of interest supplied at 1 nM (active site concentration determined by titration with E-64). Enzyme was incubated with inhibitor, present at varying concentrations, for 30 min at room temperature (21–24 °C) in 96-well microtiter plates to allow for equilibrium to be achieved for slow binding inhibitors. After preincubation, reactions were initiated with the addition of the fluorogenic substrate specified previously. The hydrolysis of this substrate yields AMC, which was monitored fluorometrically (filter pair: excitation 355 nm, emission 460 nm) using an FMAX Kinetic Microplate Reader (Molecular Devices, Sunnyvale, CA). The velocity of the cathepsin catalyzed reaction was obtained from the linear portion of the progress curves using a response factor of 275 RFU/ μ M (determined experimentally under the standard assay conditions with freshly prepared AMC stock solutions). Apparent inhibition constants, K_i' , were calculated from the velocity data generated at the various inhibitor concentrations using the software package, Batch K_i (Biokin Ltd., Pullman, WA) (25, 26). Batch K_i provides a parametric method for the determination of inhibitor potency using a transformation of the tight binding inhibition model described by Morrison (27), in which data are fitted to eq 1 where v_o is the uninhibited reaction velocity, $[E]$ is the concentration of enzyme active sites, $[I]$ is the concentration of inhibitor, and K_i' is the apparent inhibition constant.

$$v = \frac{v_o}{2[E]}([E] - [I] - K_i' + \sqrt{([E] - [I] - K_i')^2 + 4[E]K_i'}) \quad (1)$$

Progress Curve Analysis and Reversibility Assessment. The analysis of slow, tight-binding inhibitors was performed according to the method of Morrison and Walsh (28). Progress curves were measured under the standard conditions described previously. Progress curves were obtained by starting the reaction with the addition of mRab cathepsin K to assay mixtures containing substrate and CRA4. The concentration of CRA4 was varied from 0 to 250 nM. Product/time data were fitted to eq 2 in which P is the product concentration at time t , v_o is the initial rate of the substrate hydrolysis, v_s is the final steady-state rate, and k_{obs} is the apparent first-order rate constant for the transformation of the E–I complex to form the E–I* complex.

$$P = v_s t - (v_s - v_o)(1 - e^{-k_{obs}t})/k_{obs} \quad (2)$$

The reversibility of mRab cathepsin K inhibition by CRA4 was carried out by preforming the enzyme·inhibitor complex

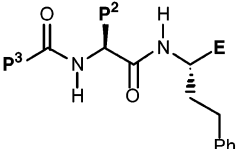
during a 1 h incubation. CRA4 was supplied at 25 μ M during the incubation phase. Following the incubation phase, the reaction was diluted 100-fold into buffer containing substrate such that the final concentration of CRA4 was 250 nM.

Crystallography and Modeling. Cathepsin K was complexed with inhibitors as previously described (20). All crystals were obtained by hanging drop vapor diffusion. For the complex with CRA3 (Table 1), crystals were obtained from 10% 2-propanol buffered with 0.1 M NaOAc, pH 4.5. For the CRA4 complex structure, crystals were grown in 6% PEG 8000 with NaK phosphate buffer, pH 6.2, and 0.2 M NaCl. Human cathepsin K/CRA1 formed diffraction-quality crystals in 16% MPD, 0.1 M Tris pH 7.0, 0.1 M MES, pH 6.0. Data for these three complexes were collected using a Raxis IV image plate with a Rigaku RU-200 generator (Table 2). A mutant of rabbit cathepsin K (29) was prepared as a potential alternative crystallizable form of the protein. Mutant rabbit cathepsin K (which provided the uncomplexed structure described herein) was crystallized from 20% MPD, 0.1 M Tris, pH 7.0 and 0.1 M MES, pH 6.0. Crystals were flash frozen in a nitrogen stream after increasing the MPD concentration to approximately 30% (while holding buffers constant). Data were collected on a single crystal at beamline 7-1 at the Stanford Synchrotron Radiation Laboratory under cryocrystallographic conditions.

Data for the three inhibitor complex structures were processed with Biotex (version 6.0, MSC, Inc.). Electron density maps were visualized using Xsight (Accelrys, Inc.). Xsight was also used to obtain molecular replacement solutions for the CRA3 and CRA4 crystal forms, using a previously determined structure of cathepsin K (without bound inhibitor and waters) as the search model (30). Refinement for the three inhibitor complexes was carried out using Xplor (31) with the X-ray target and incorporating cross validation (32). Data for the unbound structure were processed using HKL (HKL Research, Inc.). CNX (33) was used to refine the unbound cathepsin K structure using cross validation with a maximum likelihood target (34). In addition to the standard minimization, grouped temperature factor refinement, and simulated annealing scripts, the latter structure was also subjected to occupancy and individual temperature factor refinement. Comparison of the overall structures was carried out via multiple structure alignment over 215 α carbon positions using the Homology module of Insight (Accelrys, Inc.)

Ab initio calculations were performed using Hartree–Fock theory and the 6-31++G** basis set in the following manner. The systems were simplified for the calculation to include only the heterocycle and methyl ketone portion of the inhibitors (CRA3, 4, and 5). Methanethiol was added into the ketone to afford the thioacetal observed in the crystal structures. An acetamide was used to approximate the Gln 19 side chain, and a methylacetamide served as the surrogate for the Asn 158 backbone carbonyl group. The geometries of each of these individual elements were optimized independently, constraining the inhibitor/methanethiol dihedral angles and C–S bond distance to those seen in the crystal structures. The individual optimized elements were then overlaid onto the respective crystal structures (for CRA3 both rotamers about the aryl bond were utilized), and the resulting energy of the complex was calculated.

Table 1: Structure and Enzyme Activity of Selected Cathepsin Inhibitors

								
Entry	Compound No. CRA	P ³	P ²	E	CATHEPSIN K (K _i , μM)	CATHEPSIN B (K _i , μM)	CATHEPSIN L (K _i , μM)	CATHEPSIN S (K _i , μM)
a	1 [†]				--	--	--	--
b	APC 3328 (2) [†]				--	--	--	--
c	3				0.0095	2.15	0.03	--
d	4				0.0029	0.64	0.02	0.0066
e	5				0.08	9.94	0.19	0.04
f	6				0.0085	7	0.07	0.03
g	7				0.04	0.09	0.22	0.04
h	8				28.1	235	90.1	--
i	9				0.0036	0.06	0.0014	0.02
j	10				0.22	8.75	0.68	0.49
k	11				0.58	120	0.72	2.84
l	12				35	341	24	120

[†] The vinylsulfone electrophile results in irreversible inhibition of the cathepsins.

RESULTS AND DISCUSSION

Kinetic Analyses. Mutation of rabbit cathepsin K residues Tyr61 to Asp and Val157 to Leu (corresponding to the amino acid at that position in the human enzyme) yielded a protein with kinetic constants and inhibitor specificity profiles essentially equivalent to the human ortholog. For the kinetic parameter k_{cat}/K_m , the value for human cathepsin K was $5.4 \times 10^5 \text{ M}^{-1} \text{ s}^{-1}$, and the value for mutant rabbit cathepsin K was $7.6 \times 10^5 \text{ M}^{-1} \text{ s}^{-1}$. For the kinetic parameter K_m , the value for human cathepsin K was $36 \mu\text{M}$, and the value for

mutant rabbit cathepsin K was $19 \mu\text{M}$. To address inhibitor potency, the K_i' of CRA4 was measured for human cathepsin K and mutant rabbit cathepsin K under identical conditions. The K_i' of CRA4 against the human and mutant rabbit enzymes is 1.1 and 1.8 nM, respectively.

Inhibition of cathepsin K by CRA4 was determined to be time-dependent and fully reversible. Addition of cathepsin K to assay mixtures containing 74–250 nM CRA4 yielded a family of biphasic progress curves (Figure 1). This behavior is explained by the establishment of equilibria between the

Table 2: Crystallographic Data for Cathepsin K/Inhibitor Complexes

	CRA3	CRA4	uncomplexed	CRA1
space group	$P2_12_12_1$	$C2$	$P2_12_12_1$	$P2_12_12_1$
unit cell (Å)				
<i>a</i>	45.07	76.23	37.62	40.57
<i>b</i>	70.95	73.81	49.63	50.77
<i>c</i>	140.95	44.86	102.27	104.33
<i>b</i> (deg)		101.30		
molecules per asymmetric unit	2	1	1	1
X-ray source	Rigaku	Rigaku	SSRL 7-1	Rigaku
resolution (Å)	2.0	1.9	1.4	2.4
observations/reflections	61849/26168	28361/15877	529145/35829	16128/9226
completeness in highest shell (%)	60	50	87	58
R_{merge}	0.057	0.044	0.022	0.097
$R_{\text{cryst/free}}$	0.186/0.276	0.20/0.254	0.19/0.20	0.17/0.27
rms deviation bonds/angles	0.010/1.7	0.011/1.8	0.004/1.2	0.011/1.8
number of ordered waters	362	105	280	74

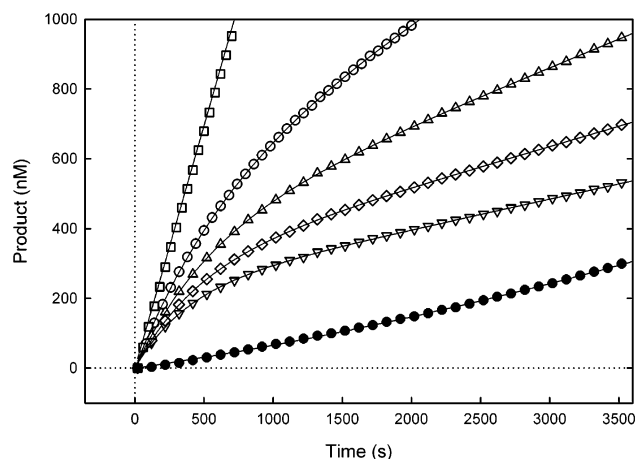


FIGURE 1: Slow-binding inhibition of mutant rabbit cathepsin K by CRA4. Progress curves were obtained by starting the reaction with the addition of substrate, 250 (∇), 167 (\diamond), 111 (Δ), 74 (\circ), and 0 (\square) nM CRA4. To address reversibility, mutant rabbit cathepsin K preincubated with 25 μ M CRA4 was diluted 100-fold into assay buffer containing substrate (\bullet). Each line represents the best fit of eq 2 to the data.

enzyme, the inhibitor, and their complexes occurring slowly as compared to equilibria involving the enzyme and substrate. The development of inhibition, which is observed experimentally as the approach to the steady-state rate, is described by eq 2 (28, 35, 36). This equation also applies to the recovery of enzymic activity that occurs upon dilution of the inhibited complex into an assay mixture containing substrate. Decay of a reversibly inhibited complex occurs until equilibrium is reached, reflected by the approach to the steady-state rate. Thus, for any given inhibitor concentration, the final steady-state rate, v_s , is independent of the direction from which equilibrium is approached. Figure 1 illustrates mRab cathepsin K progress curves in the presence of CRA4 and demonstrates the slow and reversible nature of the inhibition. Several kinetic mechanisms could be fit equally well to eq 2, and they can be distinguished by the behavior of the parameters v_0 , v_s , and k_{obs} as a function of inhibitor concentration (35, 36). The experimental data collected for the interaction between mRab cathepsin K and CRA4 conforms to a two-step slow-binding mechanism (Scheme 3) in which we observed a hyperbolic dependence of k_{obs} on CRA4 concentration. This mechanism involves

Scheme 3

Table 3: Root-Mean-Square Deviations between α Carbon Positions for Human and Mutant Rabbit Cathepsin K Structures

	CRA2	CRA3A ^a	CRA3B ^a	CRA4	mutant rabbit
cat K/CRA2		0.26	0.28	0.29	0.28
cat K/CRA3A	0.26		0.20	0.23	0.33
cat K/CRA3B	0.28	0.20		0.19	0.32
cat K/CRA4	0.29	0.23	0.19		0.30
mutant rabbit	0.28	0.33	0.32	0.30	

^a Crystal form for CRA3 complex has 2 mol/asymmetric unit, independently refined and referred to here as A and B.

an initial complex, formed by the rapid and reversible binding of the enzyme and inhibitor, followed by a slow, reversible isomerization to a more tightly bound complex.

Unbound Cathepsin K. Replacement of rabbit cathepsin K Tyr 61 with Asp and Val 157 with Leu as found in the human enzyme yields a protein with kinetic characteristics highly similar to human cathepsin K. The remaining differences between the two enzymes (human/rabbit: A1T, V5I, K77R, E92D, S152N, N154S, N180S), all far from the active site, provide a protein with slightly different surface characteristics and therefore an additional source of tractable crystal forms. These two forms of cathepsin K are very similar and directly comparable. In fact, the four structures described herein were obtained from three distinct crystal forms (Table 2), yet they superimpose with only very small deviations (Table 3). For the CRA3 structure, there is no significant difference in the positions of inhibitor atoms when the two molecules of the asymmetric unit are compared.

The structure of unbound cathepsin K provides a picture of an empty substrate-binding cleft but cannot be described as a noninhibited structure. Previous cysteine protease structures have shown that in the absence of inhibitor, the labile catalytic cysteine is easily oxidized. Most uncomplexed structures reveal the sulfur to be oxidized to the sulfonic acid (37, 38). Serendipitously, in this structure approximately two-thirds of Cys 25 is present as the sulfonic acid, while approximately one-third is found as the unusual mono-

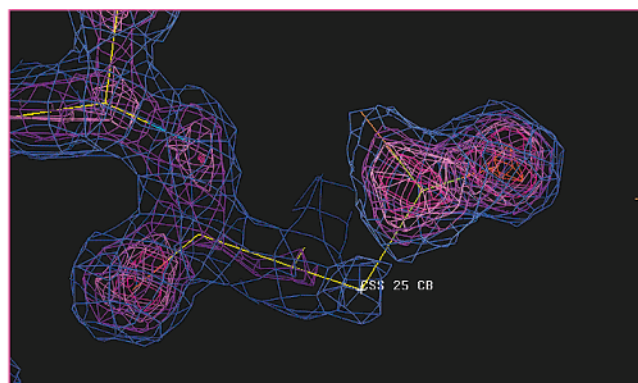


FIGURE 2: Electron density corresponding to oxidized Cys 25-S_γ. There is full occupancy of the oxygen on the right and only partial oxidation seen for the second site, on the left.

oxygenated sulfenic acid (Figure 2). There is no evidence for a third oxygen. This result provides a snapshot of an oxidation pathway that may be physiologically relevant. A recent study (39) indicated that mitigation of bone resorption following treatment of osteoclasts with nitric oxide and related molecules may be due to oxidation of Cys 25 of cathepsin K initially to the sulfenic acid and then beyond.

Inhibitor Complexes. The inhibitors described herein are comprised of a peptidic scaffold with side chains that map to positions P3 through P1' (40). Related peptidyl α -keto-heterocycles have previously been described as serine protease inhibitors with nanomolar potency (vs human neutrophil elastase) (41). CRA3, CRA4, and the previously described APC 3328 (CRA2) (30) are very similar on the nonprime side.

P3. The S3 pocket of cathepsin K is formed predominantly by Asp 61 and Tyr 67. The X-ray structures show that the P3 moieties of these inhibitors fit into a pocket defined by the side chains of Asp 61 and Tyr 67. The P3s are all heterocyclic amides or ureas: CRA2 is a piperazine urea, while CRA1 features a morpholine urea, and CRA3 and 4 have a P3 piperidine amide. All are well-tolerated in S3, although P3 is not optimized for binding in the cathepsin K S3 pocket. Consequently, it is not surprising to find different orientations of the heterocyclic ring in the four crystal structures described (Figure 3A). This is clearly a part of the inhibitor that could be changed to yield more potent and selective compounds.

P2. The P2/S2 interaction provides considerable binding potency to the small molecule cysteine protease inhibitors. The S2 binding subsite is comprised of Tyr 67 (shared with S3), Met 68, Ala 133, Leu 157, Ala 160, and Leu 205. Since S2 is a true binding pocket and well-sequestered from solvent, the right P2 group can also confer selectivity against other cysteine proteases to a small molecule inhibitor. The P2s of the inhibitors described in this paper are lipophilic with CRA1 having a P2 Tyr while the others have Leu at this position. The P2 Tyr of CRA1 superimposes well with the Leu-containing structures out to C β . The Tyr rotamer observed in this structure allows the side chain OH to be fully solvent accessible. Hydrogen bonds comparable to those that stabilize β sheet structures are formed between the amide NH of the inhibitors' P2 and the carbonyl of cathepsin K's Gly 66, between P2-CO and Gly 66- NH, and between the P1 amide NH and the Asn 158-CO (Table 4 and Figure 3B).

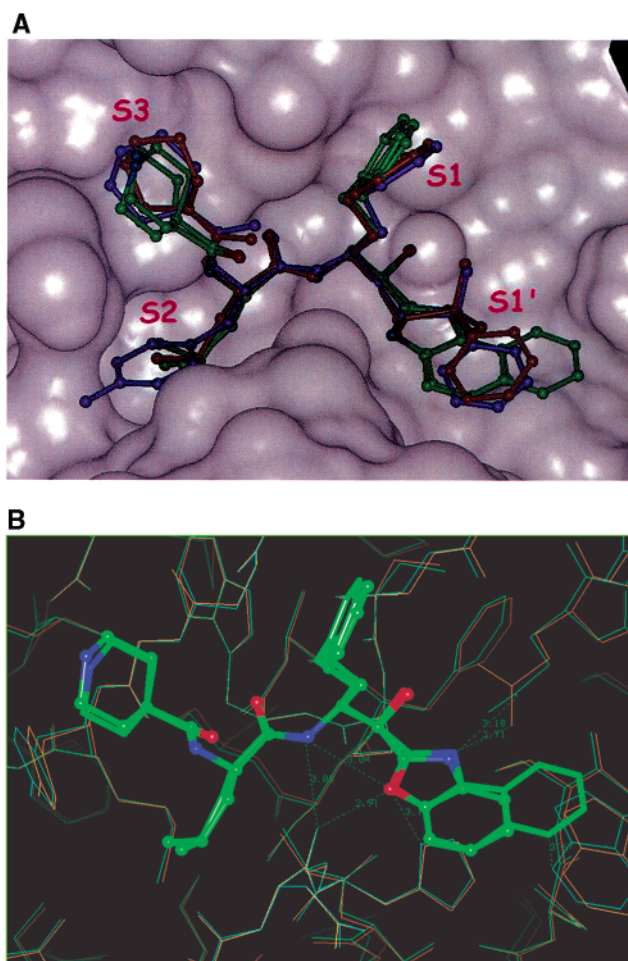


FIGURE 3: (A) Surface representation of the active site of cathepsin K, with bound inhibitors CRA2 (orange), CRA1 (purple), and CRA3 and 4 (both colored by atom type) shown and binding subsites labeled. (B) Structures of cathepsin K bound to CRA3 (cyan) and CRA4 (orange) with key hydrogen bonds shown.

P1. P1 rests in a shallow, solvent-exposed binding subsite. The P1 for all four inhibitors is homophenylalanine (Figure 3a). This side chain works well because the methylene chain avoids close contact with the carbonyl group of Gly 23, which would unfavorably contact a β - or γ -branched side chain. No particularly favorable binding interactions are made between the homophenylalanine and cathepsin K. It is not clear how P1 might be changed to improve binding or selectivity since the S1 binding pocket does not vary much among the human cathepsins.

P1'. Benzoxazole Binding in S1'. Structure determination of the complex with CRA3 revealed an ambiguity in the binding mode of the ketobenzoxazole at P1'. The heterocycle could be oriented such that either the oxazole N or the O closely approaches the P1 amide of the inhibitor and the carbonyl oxygen of Asn 158. The other oxazole heteroatom would be proximal to the side chain of Gln 19. Gln 19 is not restrained to a particular rotamer and consequently does not dictate the orientation of the benzoxazole. This binding mode differs greatly from the predicted benzoxazole binding pose of the serine protease inhibitors, in which the oxazole nitrogen is believed to form a hydrogen bond with an imidazole nitrogen of catalytic His 57 (41).

Identification of the Heterocyclic Atom that Bonds with Asn 158:O. Two compounds were synthesized to resolve the

Table 4: Relevant Hydrogen Bonding Distances at the Active Site of Cathepsin K/Inhibitor Complexes

	P1 NH to N 158 O	P2 CO to G 66 N	P2 NH to G 66 O	P1' Oe1 to H 159 Nδ1	P1' Oe1 to N 158 O	P1' Oe1 to P1 NH
cat K/CRA2	3.0	3.0	3.1	3.2 ^a	3.2 ^a	3.1 ^a
cat K/CRA3	3.2	3.0	3.0	3.2	2.7	3.0
cat K/CRA4	3.1	3.0	3.0	3.0	2.9	3.1
cat K/CRA1	3.5	3.2	3.6	3.6 ^a	3.6 ^a	3.1 ^a

^a For CRA 2 and 1, the P1' atom is a methylene carbon, not an Oe1.

Table 5: Relative Preferences of Human Cysteine Proteases for CRA 4 and 5

	CRA4/5 preference
cathepsin K	70
cathepsin L	30
cathepsin S	13
cathepsin B	24
cathepsin F	35
cathepsin V	15

ambiguity and to further characterize S1'. CRA4 and CRA5 differ from CRA3 only in the substitution of benzoxazole with either naphtho[1,2-*d*] or -[2,1-*d*]oxazole. The two naphthoxazoles can be described as isosteric but with the positions of the oxazole N and O atoms switched. These compounds were assayed versus a panel of papain-like cysteine proteases. As shown in Table 5, CRA4 was preferred by a factor of 13–70 for a panel of six cysteine proteases. The greatest preference for CRA4 over CRA5 was observed for cathepsin K. The 1.9 Å structure of the complex of cathepsin K bound to 4 reveals that the preferred orientation of the oxazole places the oxygen 2.9 Å from the carbonyl oxygen of Asn 158 and 3.1 Å from the amide nitrogen of the inhibitor P1 residue (Table 4). The hydrogen bond between Asn 158:O and P1:NH is maintained (3.1 Å). The oxazole nitrogen lies 3.1 Å from a terminal side chain atom, either Ne2 or Oe1, of Gln 19. The Gln 19 ambiguity exists for this particular complex because of a 90° rotation about χ_3 (with respect to the CRA3 structure), which orients the terminal side chain atoms such that they are approximately equidistant from the oxyanion of the bound inhibitor. Apart from this difference, the distances are very similar to those measured for the cathepsin K/CRA3 structure. The proximity of Asn 158:O to the oxazole oxygen is unexpected. This propinquity may be tolerated because of the unusual electrostatic environment at the active site of cysteine proteases. The pK_a s of Cys 25 and His 159 in the papain-like cysteine proteases are

significantly altered from normal values (42), and in the absence of substrate or inhibitor, these groups form a thiolate/imidazolium ion pair (43). While Cys 25 participates in a covalent bond in these inhibitor structures and is uncharged, His 159 may still provide a positively charged milieu to facilitate the interaction of the oxygens.

To gain insight into the binding mode displayed by these inhibitors, an *ab initio* computational study was undertaken. Comparisons of the two benzoxazole rotamers of CRA3 to each other and CRA4 with CRA5 reveal that the isomer with the oxygen of the five-membered oxazole ring closest to the carbonyl group representing Asn 158 was found to have the lower energy (the ΔE for the two rotamers of compound 3 was 5.51 kcal/mol and for CRA 4 vs CRA5 was 11.74 kcal/mol). The difference in energy between the two systems is likely due to the hydrogen bond between the acetamide (Gln 19) and the nitrogen of the CRA 4 oxazole that is not seen in the CRA3 structure due to the differing Gln 19 side chain trajectory. Examination of the structures suggests that one possible explanation for this preferred rotamer may be the dipoles of the oxazole and the oxyanion bond. In both the CRA3 and the CRA4 structures, the bond to the oxyanion eclipses one of the heteroatom bonds of the oxazole (Figure 3B). When the oxygen of the oxazole is directed away from Asn 158, it eclipses the oxyanion bond while in the observed conformation, it is antiperiplanar to it. In this latter binding mode, the dipoles of the two vicinal moieties are directed opposite to one another and thereby cancel, whereas in the former geometry they are additive and are therefore disfavored.

P1'–S1' Interactions. The crystal structures show that the benzoxazole of CRA3 and naphthoxazole of CRA4 occupy the S1' pocket of cathepsin K. The oxazole moieties lie directly over catalytic His 159 such that the oxazole oxygen is just 3.1 Å from Nδ1 of the imidazole in both structures. In the complex with CRA4, the additional aryl ring of the

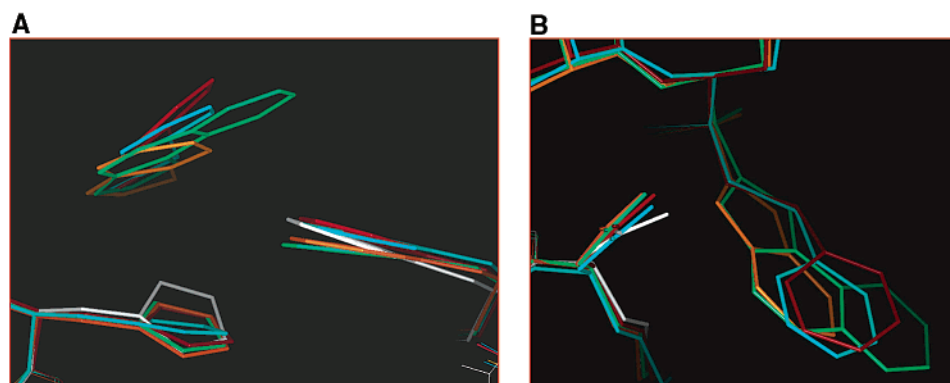


FIGURE 4: Cathepsin K/inhibitor complexes: green—CRA4; orange—CRA3; white—no inhibitor; cyan—CRA2; and red—CRA1. (A) Trp 177 adjusts to accommodate larger P1' moieties. (B) Asn 158 carbonyl rotates away from S1' in response to P1' elements.

naphthoxazole extends more deeply into the prime side, partially covering the side chain of Trp 177. The ring systems of the two inhibitors do not lie in exactly the same plane. The naphthoxazole is canted slightly upward (equivalent atoms differ in position by 0.3–0.4 Å), with respect to CRA3, as it approaches Trp 177. If it did not take a slightly different trajectory, atoms of the distal ring would closely approach Trp 177. Trp 177 also appears to have adjusted its position to more favorably approach the planar P1' elements: indole atoms on the distal edge have shifted by approximately 0.7 Å when the structures of CRA3 and 4 are compared with the P1' phenyl sulfone-containing CRA2 and CRA1 (Figure 4). Partial stacking of the 3-ring P1' element on the indole of Trp 177 may account for some of the increased potency seen for the naphthoxazole as compared with the benzoxazole when tested against cathepsins B, K, and L (Table 1).

Repositioning is also seen for main chain atoms of Asn 158. In the absence of inhibitor, the carbonyl points into S1'. In the presence of a nonbulky P1' such as methyl phenyl sulfone (CRA2 and CRA1), the carbonyl torsions away from S1'. Juxtaposition of a planar ring with Asn 158-O results in greater retreat by the latter from S1', such that the oxygen is displaced by as much as 0.7 Å when compared with the uncomplexed cathepsin K structure (Figure 4). This flexibility at the heart of the active site is most likely unnecessary during substrate catalysis but is peculiar to the nonnatural P1' constituents of these inhibitors and appears to be well-tolerated.

Exploration of Prime Side Binding. Both the benzoxazole and the naphthoxazole moieties described previously provide entry to more distal prime side binding determinants. A number of compounds were synthesized and tested against cathepsin K and related cysteine proteases to further explore the S1' pocket (Table 1). The compounds held the P3 piperidine amide, P2 leucine, and P1 homophenylalanine moieties constant with modifications of the electrophile: in general, various types of ketones. The benzoxazole (Table 1, entry c) and naphthoxazole groups (Table 1, entries d–f) clearly provide compound potency across the tested cathepsins. This observation is consistent with the previously noted preference for more electrophilic ketones as evidenced by lower LUMO energy (ketobenzoxazole < phenyl ketone and methyl ketone; cf. Table 1, entries c, h, and k, respectively) (44). This trend is also consistent with the observations that that CRA9 is preferred over CRA10, which is itself better than CRA11 (Table 1, entries i–k). Coupled to the electrophilicity differences, however, are differences in both size and geometry that affect the number and quality of van der Waals and other contacts that can be made with the enzyme. For instance, the large increase in potency of CRA9 over CRA10 might be easiest to rationalize by increased hydrophobic contacts available to CRA9. The significantly greater affinity for CRA11 over CRA8 is not explained by the LUMO energy (CRA8 < CRA11) (44); however, unfavorable geometric and steric properties of the six-membered ring may be responsible. Extension off the benzoxazole by addition of a phenyl ring was seen to improve binding to cathepsins (Table 1, entries c and d, respectively) as described previously. Additional compounds showed that hydrophobic, bulky groups are well-tolerated in the capacious S1' region (Table 1, entry f) and may be preferred over hydrophilic

groups such as sulfonamide (Table 1, entry g) except for cathepsin B. The prime side architecture of cathepsin B, however, is significantly different from the other cathepsins (38). The sulfonamide of CRA7 would extend toward His 111 of the occluding loop of cathepsin B, perhaps forming a favorable hydrogen bond with the imidazole. The side chain of Asn 158 that forms most of the proximal wall of S1' in many of the cathepsins is replaced in cathepsin B by Gly and a dramatic change in strand direction, which would have an impact on binding of P1' moieties directed toward this side of S1'. Removing the electrophilic carbon yielded a minimally active compound (CRA12, Table 1, entry l). Other substitutions off the two or three ring examples presented here could clearly be useful for increasing potency and for gaining selectivity in the context of a drug discovery program.

ACKNOWLEDGMENT

We thank Dr. John O. Link for helpful comments. Portions of this research were carried out at the Stanford Synchrotron Radiation Laboratory, a national user facility operated by Stanford University on behalf of the U.S. Department of Energy, Office of Basic Energy Sciences. The SSRL Structural Molecular Biology Program is supported by the Department of Energy, Office of Biological and Environmental Research and by the National Institutes of Health, National Center for Research Resources, Biomedical Technology Program, and the National Institute of General Medical Sciences.

REFERENCES

1. Bossard, M., Tomaszek, T., Thompson, S., Amegadzie, B., Hanning, C., Jones, C., Kurdyla, J., McNulty, D., Drake, F., Gowen, M., and Levy, M. (1996) *J. Biol. Chem.* 271, 12517–12524.
2. Delaisse, J.-M., Boyde, A., Maconnachie, E., Ali, N. N., Sear, C. H. J., Eeckhout, Y., Vaes, G., and Jones, S. J. (1987) *Bone* 8, 305–313.
3. Everts, V., Beertsen, W., and Schröder, R. (1988) *Calcif. Tissue Int.* 43, 172–178.
4. Gelb, B., Shi, G.-P., Chapman, H., and Desnick, R. (1996) *Science* 273, 1236–1238.
5. Inui, T., Ishibashi, O., Inaoka, T., Origane, Y., Kumegawa, M., Kokubo, T., and Yamamura, T. (1997) *J. Biol. Chem.* 272, 8109–8112.
6. Saftig, P., Hunziker, E., Everts, V., Jones, S., Boyde, A., Wehmeyer, O., Suter, A., and von Figura, K. (2000) *Adv. Exp. Med. Biol.* 477, 293–303.
7. Gowen, M., Lazner, F., Dodds, R., Kapadia, R., Field, J., Tavaría, M., Bertonecello, I., Drake, F., Zavorselk, S., Tellis, I., Hertzog, P., Debouck, C., and Kola, I. (1999) *J. Bone Miner. Res.* 14, 1654–1663.
8. Barrett, A. J., and Hanada, K. (1982) *Biochem. J.* 201, 189–278.
9. Palmer, J. T., Rasnick, D., Klaus, J. L., and Brömme, D. (1995) *J. Med. Chem.* 38, 3193–3196.
10. Brömme, D., Klaus, J. L., Okamoto, K., Rasnick, D., and Palmer, J. T. (1996) *Biochem. J.* 315, 85–89.
11. Dai, Y., Hedstrom, L., and Abeles, R. (2000) *Biochemistry* 39, 6498–6502.
12. Smith, R., Bhargava, A., Browe, C., Chen, J., Dumas, J., Hatoum-Mokdad, H., and Romero, R. (2001) *Bioorg. Med. Chem. Lett.* 11, 2951–2954.
13. Marquis, R., Yamashita, D., Ru, Y., Lo Castro, S., Oh, H., Erhard, K., Des Jarlais, R., Head, M., Smith, W., Zhao, B., Janson, C., Abdel-Meguid, S., Tomaszek, T., Levy, M., and Veber, D. (1998) *J. Med. Chem.* 41, 3563–3567.
14. Fenwick, A., Gribble, A., Ife, R., Stevens, N., and Witherington, J. (2001) *Bioorg. Med. Chem. Lett.* 11, 199–202.

15. Duffy, K., Ridgers, L., Des Jarlais, R., Tomaszek, T., Bossard, M., Thompson, S., Keenan, R., and Veber, D. (1999) *Bioorg. Med. Chem. Lett.* 9, 1907–1910.
16. Bossard, M., Tomaszek, T., Levy, M., Ijames, C., Huddleston, M., Briand, J., Thompson, S., Halpert, S., Veber, D., Carr, S., Meek, T., and Tew, D. (1999) *Biochemistry* 38, 15893–15902.
17. Marquis, R., Ru, Y., Lo Castro, S., Zeng, J., Yamashita, D., Oh, H., Erhard, K., Davis, L., Tomaszek, T., Tew, D., Salyers, K., Proksch, J., Ward, K., Smith, B., Levy, M., Cummings, M., Haltiwanger, R., Trescher, G., Wang, B., Hemling, M., Quinn, C., Cheng, H., Lin, F., Smith, W. W., Janson, C., Zhao, B., McQueney, M., D'Alessio, K., Lee, C., Marzulli, A., Dodds, R., Blake, S., Hwang, S., James, I., Gress, C., Bradley, B., Lark, M., Gowen, M., and Veber, D. (2001) *J. Med. Chem.* 44, 1380–1395.
18. Falgouty, J., Oballa, R., Okamoto, O., Wesolowski, G., Aubin, Y., Rydzewski, R. M., Prasit, P., Riendeau, D., Rodan, S., and Percival, M. (2001) *J. Med. Chem.* 44, 94–104.
19. Altmann, E., Renaud, J., Green, J., Farley, D., Cutting, B., and Jahnke, W. (2002) *J. Med. Chem.* 45, 2352–2354.
20. Linnevers, C., McGrath, M., Armstrong, R., Mistry, F., Barnes, M., Klaus, J., Palmer, J., Katz, B., and Bromme, D. (1997) *Protein Sci.* 6, 919–921.
21. Brömme, D., and McGrath, M. E. (1996) *Protein Sci.* 5, 789–791.
22. Somoza, J. R., Zhan, H., Bowman, K. K., Yu, L., Mortara, K. D., Palmer, J. T., Clark, J. M., and McGrath, M. E. (2000) *Biochemistry* 39, 12543–12551.
23. Ho, J. D., Meltser, Y., Buggy, J. J., Palmer, J. T., Elrod, K., Chan, H., Mortara, K. D., and Somoza, J. R. (2002) *Acta Crystallogr., Sect. A*, in press.
24. Fehrentz, J., and Castro, B. (1983) *Synthesis*, 678.
25. Kuzmic, P. (1996) *Anal. Biochem.* 237, 260–273.
26. Kuzmic, P., Sideris, S., Cregar, L., Elrod, K., Rice, K., and Janc, J. (2000) *Anal. Biochem.* 281, 62–67.
27. Morrison, J. (1969) *Biochim. Biophys. Acta* 185, 269–286.
28. Morrison, J., and Walsh, C. (1988) *Adv. Enzymol.* 61, 201–301.
29. Tezuka, K., Tezuka, Y., Maejima, A., Sato, T., Nemoto, K., Kamioka, H., Hakeda, Y., and Kumegawa, M. (1994) *J. Biol. Chem.* 269, 1106–1109.
30. McGrath, M., Klaus, J., Barnes, M., and Bromme, D. (1997) *Nat. Struct. Biol.* 4, 105–109.
31. Brünger, A. (1990) *X-PLOR Manual, Version 3.1: A system for X-ray crystallography and NMR*, Yale University, New Haven, CT.
32. Brünger, A. (1992) *Nature* 355, 472–474.
33. Brünger, A., Adams, P., Clore, G., DeLano, W., Gros, P., Grosse-Kunstleve, R., Jiang, J.-S., Kuszewski, J., Nilges, M., and Pannu, N. (1998) *Acta Crystallogr., Sect. D* 54, 905–921.
34. Pannu, N., and Read, R. (1996) *Acta Crystallogr., Sect. A* 52, 659–668.
35. Cha, S. (1975) *Biochem. Pharmacol.* 24, 2177–2185.
36. Cha, S. (1976) *Biochem. Pharmacol.* 25, 1561.
37. Kamphuis, I., Kalk, K., Swarte, M., and Drenth, J. (1984) *J. Mol. Biol.* 179, 233–256.
38. Musil, D., Zucic, D., Turk, D., Engh, R. A., Mayr, I., Huber, R., Popovic, T., Turk, V., Towatari, T., and Katunuma, N. (1991) *EMBO J.* 10, 2321–2330.
39. Percival, M., Ouellet, M., Campagnolo, C., Claveau, D., and Li, C. (1999) *Biochemistry* 38, 13574–13583.
40. Schechter, I., and Berger, A. (1967) *Biochem. Biophys. Res. Commun.* 27, 157–162.
41. Edwards, P., Wolanin, D., Andisik, D., and Davis, M. (1995) *J. Med. Chem.* 38, 76–85.
42. Mellor, G., Thomas, E., Topham, C., and Brocklehurst, K. (1993) *Biochem. J.* 290, 289–296.
43. Polgar, L. (1974) *FEBS Lett.* 47, 15–18.
44. Chan, A., and Golec, J. (1996) *Bioorg. Med. Chem.* 4, 1673–1677.

BI035041X